Supporting Information

Spin-Polarized Photon Emission by Resonant Multipolar Nanoantennas

Sergey S. Kruk,[1] Manuel Decker,[1] Isabelle Staude,[1] Stefan Schlecht,[1] Michael Greppmair,[1] Dragomir N. Neshev,[1,] and Yuri S. Kivshar[1]*

[1]Nonlinear Physics Centre and Centre for Ultrahigh Bandwidth Devices for Optical Systems (CUDOS), Research School of Physics and Engineering, Australian National University, Canberra ACT 0200, Australia

SI includes:

9 pages

7 figures, and

2 tables.

Split-ring resonators: resonances and multipole contributions

We numerically simulate spectra of SRRs on a glass substrate covered with MgF_2 using geometrical dimensions obtained from SEM images. We use a semi-infinite substrate with refractive index of $n = 1.41$ with golden SRRs on top, covered with 12-nm-thin MgF_2 with refractive index $n = 1.38$. For the permittivity of gold we use data from Johnson and Christy [1]. The split-ring resonators (SRRs) are characterized by several resonances (*fundamental resonance, resonance 1, resonance 2, and resonance 3)* which can be excited by specific (linear) polarization states of (plane wave) excitation (see Fig. S1).

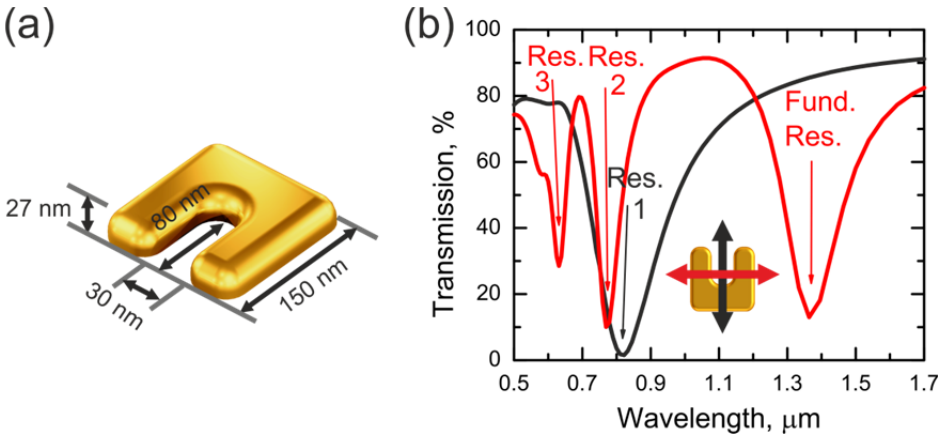

Figure S1. (a) Geometry of the SRR used in experiments and simulations. (b) Numerically calculated transmission spectra of an array of SRRs indicating the fundamental and higher order resonances for two orthogonal linear polarizations, shown with red and blue curves, respectively.

For vertical polarization [black line] the spectrum is characterized by a single broad resonance centered at approximately $\lambda_1 = 815$ nm (*resonance 1*). This resonance is commonly referred to as the (first-order) electric resonance due to its strong electric-dipole moment along y-direction. Since *resonance 1* is dominated by the electric-dipole moment its contributions to the generation of spin-polarized emission of photons is small [see Figure S4(b,c)]. For horizontal polarization [red line] three resonances at λ_f=1400 nm (*fundamental resonance*), $\lambda_2 = 760$ nm (*resonance 2*) and $\lambda_3 = 620$ nm wavelength (*resonance 3*) can be found.

The resonances 2 & 3 are often referred to as the higher-order resonances of a SRR. Following Mühlig *et al.* [2], we identify the characteristics of *resonance 2* in terms of the relevant multipole moments: it is characterized by a superposition of an electric dipole along *x* direction, an electric quadrupole with two non-zero components $Q_{xy} = Q_{yx}$, and a weak magnetic-dipole moment along *z* direction. The total scattering/extinction of the SRR at around 800 nm wavelength is therefore dominated by electric dipole and electric quadrupole contributions. For *resonance 2* the fields from the electric-dipole and the electric-quadrupole components are perpendicular to each other and $\pi/2$ phase-shifted [see Fig. 1(b)], hence, *resonance 2* of our SRR nanoantenna is well-suitable for generation of spin-polarized emission of photons.

The fundamental resonance of a SRR has a circulating current around the metal loop [see also Fig. 4(a)] and is characterised by a strong electric dipole moment **p** in *x* direction and a weaker (but comparable) magnetic dipole moment **m** in *z* direction. This makes it siutable for a generation of a spin-polarized emission. However, we numerically find (see Supplementary

Figure S4(a,d)] that in our design the effect of spin-polarized emission is more pronounced for *resonance 2*. More importantly, the use of higher-order resonances allows for operation in the visible spectral range.

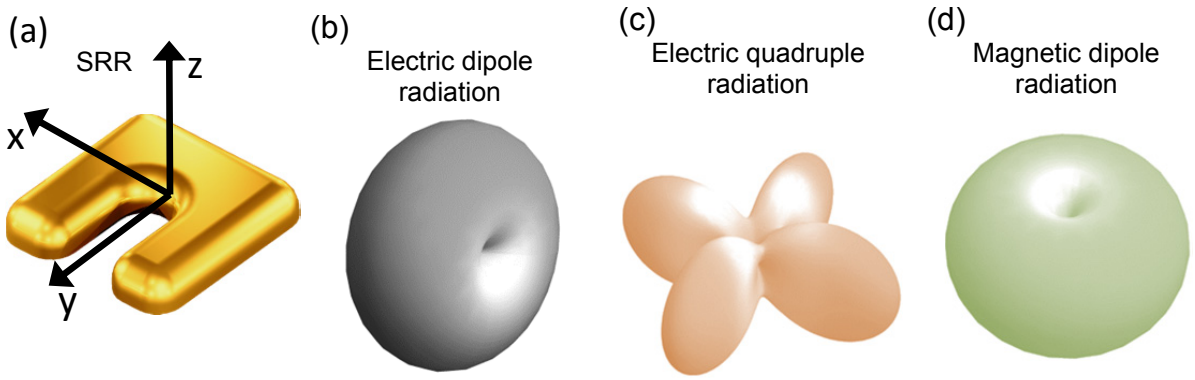

Figure S2. (a) Orientation of the SRR and (b-d) the corresponding 3D radiation patterns of the three dominant multipole moments present in *resonance 2*.

Scanning electron-microscope (SEM) images of the experimental structures as well as the raw transmittance measurements are shown in Fig. S3 and are in good agreement with the numerical calculations shown in Fig. S1(b).

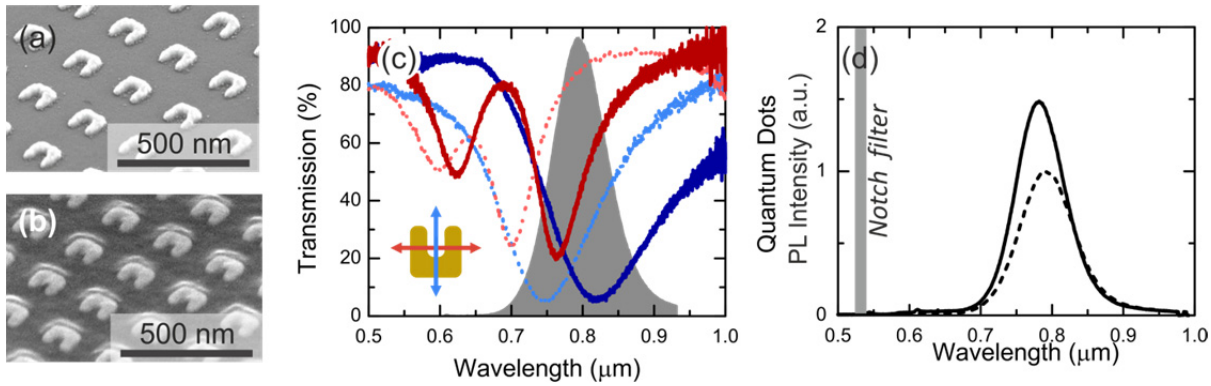

Figure S3. (a) SEM image of fabricated SRR array on glass substrate. (b) SEM image of a SRR array covered with a 12-nm-thin MgF_2 spacer and a layer of QDs (not seen due to their low contrast with MgF_2). (c) Transmission spectra of the SRR array on a bare glass substrate (light dotted lines) and the SRRs on glass covered with the MgF_2 layer and QDs (dark solid colors). The spectra are shown for two principle linear polarizations: horizontal (red) and vertical (right). Grade shaded area shows photoluminescence spectrum of quantum dots. (d) PL spectra of QDs on MgF_2 spacer above SRRs (solid curve) and above the glass substrate with MgF_2 spacer layer (dashed curve).

Localized dipole excitation scenarios

By performing numerical simulations using CST Microwave studio we explore the possibility to generate spin-polarized light. In our calculations we substitute the QDs by an electric dipole source (dipole antenna of a small size) pointing in *x*, *y*, or *z* direction.

Figure S4 shows the numerically calculated current distribution within the SRR and the ellipticity of the emission for different orientations of the localized dipole source placed above the SRR and MgF_2 spacer. Because of the symmetry of the modes (see current distributions in the top row of Fig. S4) different orientations of the dipole source excite different resonances in SRR.

When the dipole moment is pointing in *x*-direction, the *fundamental resonance* of the SRR is excited for $\lambda \approx 1400$ nm. For the two remaining dipole orientations the fundamental mode can't be excited. Figure S4(a) shows the calculated current distribution in a SRR for this scenario. In agreement with previous studies [2-4], we observe a single loop of current in the SRR which gives rise to both an electric- and a magnetic-dipole response simultaneously.

For *resonance 1* and *2* the excitation scenario for the different modes is slightly more complicated since they are spectrally overlapping at $\lambda \approx 800$ nm. At this wavelength, *resonance 1* is predominantly excited for dipole-orientations in *y* and *z* direction leading to the corresponding current distributions shown in Fig. S4(b,c) while for *x* orientation resonance 2 is excited. We calculate the current distributions for the three cases of excitation with the dipoles pointing in three orthogonal orientations as shown in Fig. S4(b-d).

For all cases, we then calculate the polarization-state of emission with regard to ellipticity [second row in Fig. S4(a-d)] and find circularly-polarized emission for all cases, however, we find that the effect of circular emission is most pronounced for the *resonance 2* resulting in purely circularly polarized light for emission for specific *k*-vectors [second row in Fig. S4].

Since, in experiment, the orientation of the QDs is randomly distributed and the dipole emission is centred around 800 nm wavelength, only modes within the spectral range of QD emission are excited (*resonance 1* and *2*). Thus, in our work we focus on the higher order *resonance 2* of the SRRs [Fig. S4(b-d)], which is shifted towards the visible part of the spectrum and is in spectral overlap with the QD emission. Nevertheless, for an appropriate choice of emitter, the fundamental resonance at $\lambda_0 \approx 1400$ nm also supports the superposition of the strong electric- and magnetic-dipole moments that is necessary for the generation of spin-polarized light emission [see Fig. S4(a)].

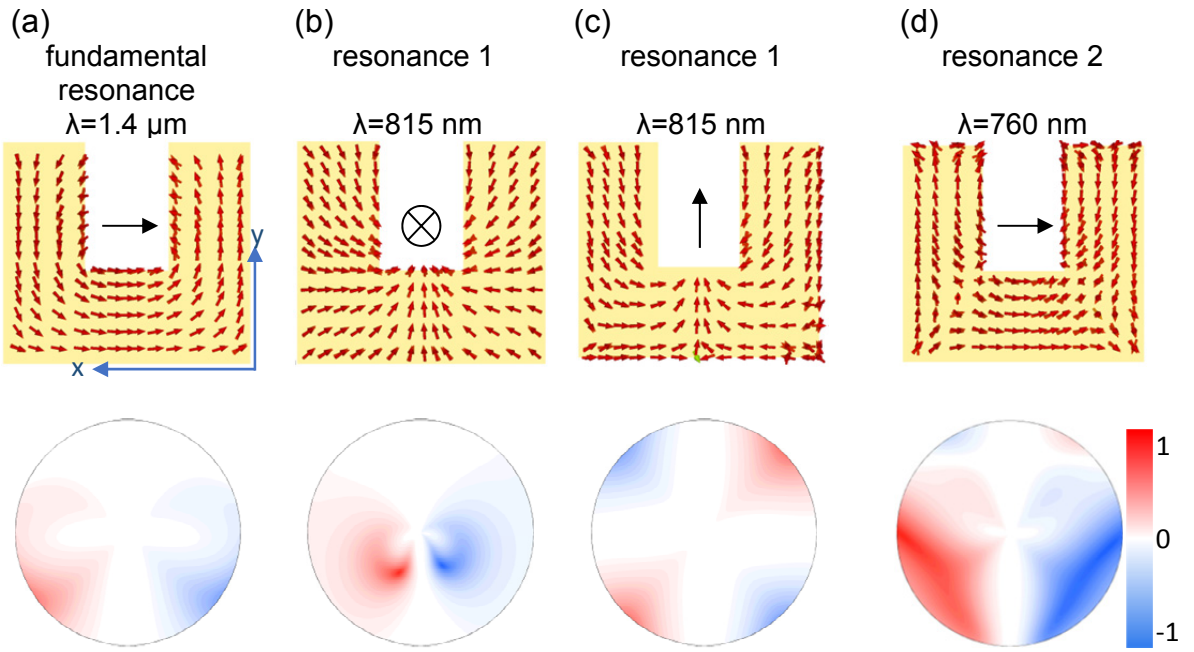

Figure S4. Calculated current distributions within the SRR (top row) and ellipticity of the emission as seen from the detector side (bottom row) for different excitation wavelength and orientations of the dipole source (black arrow in the top row).

We further investigate how the generation of spin-polarized light is affected by the positioning the emitter in a fixed plane above the SRR. Since we are interested in the emission characteristics of *resonance 2* we consider *x*-orientation of the emitter [see Fig. S4(d)]. As the distance between the SRR and the emitter in *z*-direction is fixed by thickness of the spacer layer, we vary *x*- and *y*-coordinates of the emitter only. To evaluate the impact of a particular spatial position of a dipole on the efficiency of the generation of spin-polarized light we introduce a Figure of Merit (FOM):

$$FOM(x,y) = \frac{\oiint I(x,y,\varphi,\theta)\cdot|\varepsilon(x,y,\varphi,\theta)+\varepsilon(-x,y,\varphi,\theta)|d\varphi d\theta}{\oiint I(x,y,\varphi,\theta)d\varphi d\theta} \quad \text{(S1)}$$

where *x,y* define the position of the emitter with respect to the centre of SRR, φ,θ define the direction of emission [see Fig. 5 (a)], I is the intensity of emission, and ε is the ellipticity [$\varepsilon = \tan(\chi)$]. In this equation $|\varepsilon(x,y,\varphi,\theta)+\varepsilon(-x,y,\varphi,\theta)|$ reflects the mirror symmetry plane of the SRR.

Figure S5 (b) shows the FOM for different positions of the emitter in the *x*-*y* plane. As one can see, *the dominant contribution for spin-polarized emission originates from the emitters positioned close to centre of a SRR*. Qualitatively, for emitters displaced in *y*-direction the FOM rapidly decreases, nevertheless the effect of spin-polarized emission shown in Fig. S4(d) is qualitatively preserved. For emitters displaced in *x*-direction the effect mostly cancels for +*x*-shift and -*x*-shift due to the symmetry properties of the SRR symmetry, hence, resulting in a low FOM as well.

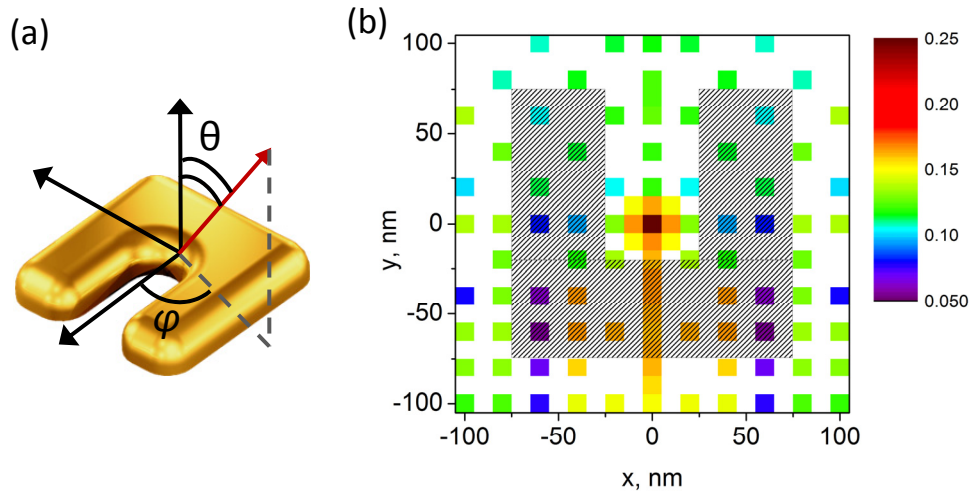

Figure S5. (a) φ,θ angles used in Eq. S1. (b) Figure of Merit for different positions (colored dots) of the emitter. Dashed region shows position of the SRR antenna.

Fabrication

In order to experimentally demonstrate spin-polarized emission of photons we couple semiconductor QDs to our SRR nanoantennas, thereby driving the antenna by near-field interaction. We fabricate gold SRRs in a periodic lattice with the lattice constant of a = 300 nm by standard electron-beam lithography on a 1-mm-thin glass substrate coated by 5 nm of Indium-Tin-Oxide (ITO), followed by the evaporation of 27 nm of gold and a lift-off procedure. Next, we cover the SRRs by a 12-nm-thin MgF_2 spacer layer using sputtering. A uniform layer of core-shell QDs (CdSeTe core with a shell of ZnS and polymer coating: 10 μl of 2.2 μM Invitrogen Qdot®800 ITK^{TM} streptavidin conjugate, quantum yield q= 56% (lot data), diluted in 500 μl Invitrogen Qdot®800 incubation buffer) is then spin-coated on top of the MgF_2 spacer layer (1500 rpm, 30 s). The concentration of QDs in the buffer solution and the parameters of spin-coating were optimized in order to keep the surface density of QDs close the surface density of SRRs (1 SRR per 0.09 μm^2 area). This fabrication approach leads to a randomized positioning of the QDs in a plane 12 nm above the SRRs and also naturally results in a fraction of QDs not being coupled to the SRRs. However, the uncoupled quantum dots do not influence the effect of spin-polarized emission since, on average, they emit an equal amount of photons with opposite spins. The thickness of the MgF_2 layer was chosen to both prevent quenching of the QDs and to achieve good coupling between the QDs and the SRRs. SEM images of fabricated SRRs before and after coating by MgF_2 and QDs are shown in Figs. S3(a,b).

Experimental setup for back-focal plane measurements

To excite the QDs we use a 532 nm solid-state, diode-pumped, Nd-YVO_4 laser with frequency doubling. The laser light is transmitted through a 532 nm-wavelength band pass filter which cuts out the traces of the pump laser diode at 808 nm and of the fundamental lasing wavelength at 1064 nm. The laser light then passes through a 10x (NA=0.25) microscope objective and illuminates a spot with a diameter of around 100 µm – the laser focus is positioned at the centre of 100x100 µm SRRs array. The emission of the SRRs

coupled to the QDs is collected by a second 50x (NA=0.8) objective that is positioned at its focal distance with respect to the sample. The numerical aperture of the second objective was chosen such that it allows collecting all the emission coming from the substrate side. The maximum collection angle of the emission is limited by total internal reflection in a glass substrate and is about 44 degrees. After the second objective, a 532 nm-wavelength notch filter cuts out the laser light and transmits the QD emission only.

A pair of an achromatic quarter-wave plate and a linear polarizer is used to select each of the six polarization states, required for the extraction of the Stokes coefficients [see Eqs. S1]. A lens is used to project the image from the back-focal plane of the second objective onto the CCD camera.

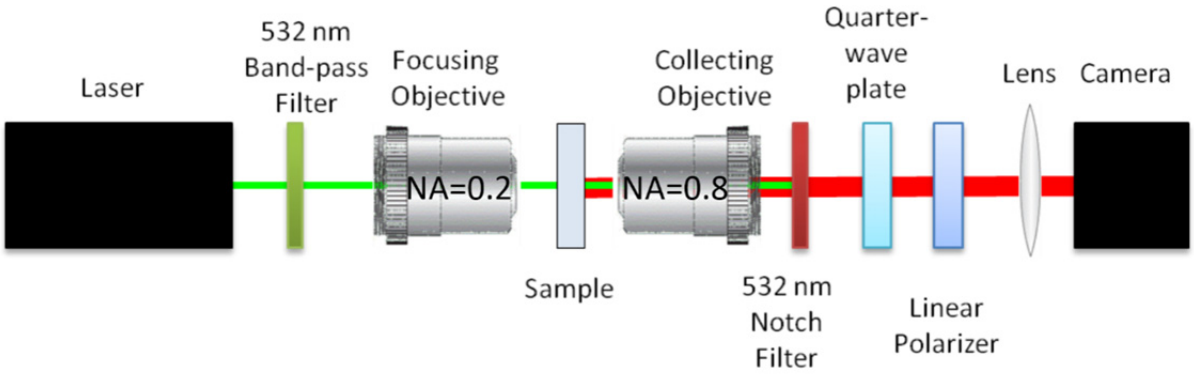

Figure S6. Experimental setup used for back-focal plane imaging of the QD emission.

Stokes coefficients

The Stokes coefficeints provide a complete description of the polarization state of light in terms of its *total intensity* I_{tot}, (fractional) *degree of polarization* ρ, *polarization inclination angle* ψ, and the *ellipticity angle* χ. The ellipticity $\tan(\chi)$ is defined as the ratio of the two axes of the polarization ellipse (see Fig. S7), and the polarization inclination is described by the angle between the main polarization axis and the *x*-axis of the laboratory coordinate system.

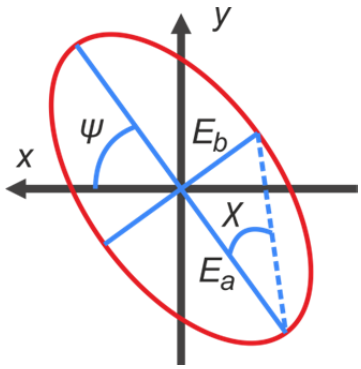

Figure S7. Schematic of the polarization ellipse with the Stokes coefficients of ellipticity angle χ and polarization-inclination angle ψ. E_a and E_b are the main polarization axes (solid blue lines) of the polarization ellipse.

Experimentally, we find the Stokes parameters by measuring the total intensity $I(\theta, \varphi)$, where θ is the angle between the direction of the linear polarizer's axis and the *y*-axis of our laboratory coordinate system. φ is the extra phase delay between the two orthogonal linear components of the electric field of the incident wave, that is introduced by the quarter-wave plate. The measured Stokes parameters in the back-focal plane are then given by

$$\begin{aligned} S_0 &= I(0^o, 0) + I(90^o, 0) = I_{tot} \\ S_1 &= I(0^o, 0) - I(90^o, 0) = \rho\, I_{tot}\, \cos 2\psi \cos 2\chi \\ S_2 &= I(45^o, 0) - I(135^o, 0) = \rho\, I_{tot}\, \sin 2\psi\, \cos 2\chi \\ S_3 &= I\left(45^0, \frac{\pi}{2}\right) - I\left(135^o, \frac{\pi}{2}\right) = \rho\, I_{tot}\, \sin 2\chi \end{aligned} \tag{S2}$$

and the evaluation of the experimental results is shown in Table 1. Remarkably, the Stokes parameters S_1-S_3 already give a clear indication that the polarization state of the radiation emitted from the QD-SRR system exhibits elliptically polarized emission which is strongly dependent of the direction of emission. Using the experimentally measured parameters we then extract the coefficients ρ, ψ, χ using Eqs. (S1). Table 2 summarizes the resulting Stokes coefficients. The maximum/minimum polarization-inclination angle measured was ±45 degrees and maximum/minimum ellipticity (ratio of the main axes of polarization ellipse) was ±0.5.

Table S1. Stokes parameters

	Polarizations used for retrieval	parameter, resolved in *k*-space
S_0	+	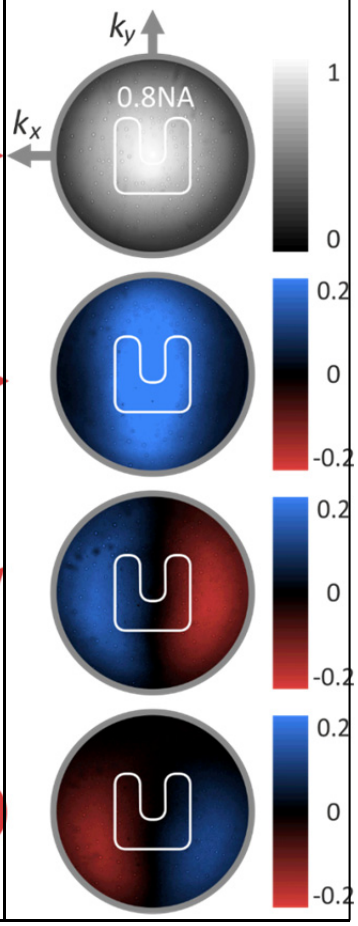
S_1	−	
S_2	−	
S_3	−	

Table S2. Stokes coefficients

Total Intensity, a.u.	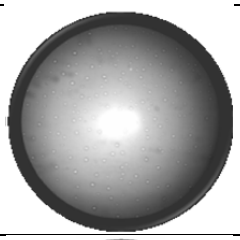
Degree of Polarization Max 15% Ave 11%	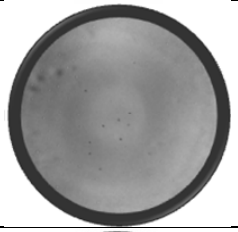
Polarization inclination angle ψ Max/Min ±45°	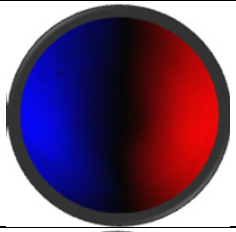
Ellipticity $Tan(\chi)=E_b/E_a$ Max/Min ±0.5	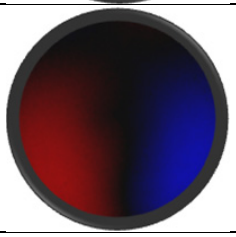

References

1. P. B. Johnson and R. W. Christy, "Optical constants of the noble metals," Phys. Rev. B 6, 4370-4379 (**1972**).
2. Mühlig, S.; Menzel, C.; Rockstuhl, C.; Lederer, F. *Metamaterials* **2011,** 5, 64-73.
3. von Cube, F.; Irsen, S.; Niegemann, J.; Matyssek, C.; Hergert, W.; Busch, K.; Linden, S. *Opt. Mater. Express* **2011,** 1, (5), 1009-1018.
4. von Cube, F.; Irsen, S.; Diehl, R.; Niegemann, J.; Busch, K.; Linden, S. *Nano Lett.* **2013,** 13, (2), 703-708.